RSC Advances

ROYAL SOCIETY OF CHEMISTRY

www.rsc.org/advances

Vapor hydration of a simulated borosilicate nuclear waste glass in unsaturated conditions at 50°C and 90°C

A. Ait Chaou[a*], A. Abdelouas[a], Y. El Mendili[a], R. Bouakkaz[a], S. Utsunomiya[b], C. Martin[c], X. Bourbon[c]

[a] SUBATECH, UMR 6457CNRS-IN2P3, Ecole des Mines de Nantes, Université de Nantes, 4 rue Alfred Kastler, BP 20722, 44307 Nantes cedex 03, France.

[b] Department of Nuclear Engineering and Management, School of Engineering, The University of Tokyo, 7-3-1 Hongo, Bunkyo-ku, Tokyo 113-8656, Japan

[c] French National Radioactive Waste Management Agency (ANDRA), 1/7, rue Jean Monnet, Parc de la Croix-Blanche, 92298 Châtenay-Malabry Cedex, France.

Abstract

Vapor hydration of a simulated typical French nuclear intermediate-level waste (ILW) glass in unsaturated conditions has been studied in order to simulate its behaviour under repository conditions before complete saturation of the disposal site. The experiments were conducted for one year at 50 °C and 90 °C and the relative humidity (RH) was maintained at 92% and 95%.

The glass hydration was followed by Fourier Transform Infra-Red spectroscopy (FTIR). The surface of reacted glass was characterised by scanning electron microscopy (SEM) and Transmission Electron Microscopy (TEM). The chemical and mineralogical composition of the alteration products were studied by Energy Dispersive X-ray Spectroscopy (EDS) and μ-Raman spectroscopy, respectively. The glass hydration increased with temperature and RH and led to the formation of a depolymerized gel layer depleted in alkalis.

The glass hydration rate decreased with time and remained almost unchanged for the last three months of time exposure. Overall, the ILW glass hydration rate was similar to that obtained with the SON68 high-level waste glass.

Keywords: Vapor hydration, geological disposal, nuclear glass

*: corresponding author (aitchaou@subatech.in2p3.fr)

1. Introduction

In France borosilicate glasses have been considered for high-level and certain intermediate-level waste confinement. Final geological disposal in a deep and stable rock seems to be the best option to guarantee safety over a long period of time. Accordingly, in France the nuclear waste forms are expected to be disposed in Callovo-Oxfordian claystone.

When in contact with an aqueous solution and/or humid air environment, borosilicate glass is subjected to chemical attack that results in progressive alteration of the glass matrix. Constituent elements of the glass dissolve into solution, elements initially in the solution diffuse into or are absorbed onto the solid and new phases may appear. These processes lead to the formation of surface layers on the corroded glass. Dissolution kinetics of HLW borosilicate glasses in pure water, but also in clayey groundwater have been extensively studied in the litterature [1–8]. As regards alteration of nuclear glasses, in particular the French inactive SON68 glass, in aqueous media, dedicated studies have allowed to identify several alteration steps characterized by different mechanisms: interdiffusion, alteration at the maximal alteration rate (r_{hydr0}), slowdown of the alteration rate and a residual alteration rate (r_r). Studies of the alteration kinetics of nuclear glasses have long attributed the observed slowdown in the rate to chemical affinity mechanisms (affinity laws) [9–11]. However, this theory has been called into question [12–14]. The mechanism currently taken into consideration by the CEA is the development of a protective gel forming a diffusion barrier for reactive species [15, 16]. Silicon retention within the gel is also considered to be one of the parameters affecting the protective properties of the gel layer [17].

Studies have also been conducted on ILW borosilicate glass alteration in cementitious medium [18, 19]. Depierre et al. [18, 19] studied the influence of Ca-enriched solution and its influence on glass alteration mechanisms and kinetics and the Ca–Si interaction processes. The authors suggest that four main mechanisms control the glass durability depending on the pH, the reaction progress and the Ca concentration. The authors shown that Ca-enriched solution presents antagonist effects according to the relative importance of these parameters. Strong similarities were noted between glass alteration in Ca rich high-pH solution and cement hydration. The characterization to determine the properties of the thin passivating layer formed at the glass or cement grain surface, which is assumed to account for the rate-limiting step, is a technical challenge today [20, 21]. Depierre et al. [19] shows that three main factors affect the glass dissolution rate: SA/V, the pH and the Ca concentration in solution.

The Ca concentration is the most important parameter controlling the growth rate and also the growth mode of C–S–H [22, 23].

Under deep geological disposal conditions, vapor hydration may be also an important corrosion process of both HLW and ILW nuclear waste glasses in a hydrologically unsaturated geological repository [24]: i) the hydrogen production induced by the anoxic corrosion of metallic components in HLW disposal cells is likely to prevent a fast resaturation of the voids within the waste packages; ii) during the operating period of the ILW disposal zone (up to 100 years), concrete components (waste disposal packages, concrete vaults…) will be ventilated in order to guarantee operating safety and to contribute to the evacuation of residual heat from the waste. In the two cases, the resaturation process will then be very slow and as a consequence, glass vapor hydration may occur before the porewater has completely infiltrated the container. However, only a few studies were dedicated to glass vapor hydration [25-31]. Recent papers on the vapor hydration of borosilicate glasses have been published by McKeown *et al.*[32, 33] and Buechele et *al.*[34]. The authors used state-of-art spectroscopic techniques to investigate glass alteration layer. Hence, Raman and X-ray absorption spectroscopic studies showed that, at high temperature (200°C) and short time periods (3-20 days), the major hydration product is a depolymerized hydrated altered glass with some crystals of analcime and leucite. Furthermore, Buechele *et al.*[34] and McKeown et al.[33] found that during vapor hydration tests of a Technetium-doped glass, Tc^{7+} was largely reduced into highly immobile Tc^{4+}.

In the presence of vapor water, an aqueous film is formed on the glass surface, whose thickness depends on the relative humidity, the composition of the glass and its surface condition. The alteration of glass by vapor water leads also to rapid precipitation of secondary phases, but the thickness of hydrated glass is lower compared to the alteration in the liquid water [28]. According to the studies carried out on the alteration kinetics of U.S. nuclear glasses by water vapor, the alteration can not begin to relative humidities below 50% [27]. Abrajano et al. [28] showed that alteration of SRL 131 glass is negligible for a relative humidity of 70%, even at a temperature of 202 °C. In general, the number of layer of water adsorbed on the glass surface changes slightly depending on the relative humidity to about 80-90% and then increase sharply from 90% leading to a maximum glass hydration [25, 26]. For this reason, we chose for this study to work under 92% and 95% of relative humidity.

In this work, we studied the vapor hydration of a simulated French ILW nuclear glass under unsaturated conditions and we studied how the exposure to water vapor changes the chemical and / or physical characteristics of glass surface. The hydration kinetics and the alteration layers were studied. We chose to study both relative humidity 92% and 95% based on the results of the previous studies and two temperatures 50°C and 90°C, expected under disposal conditions.

2. Materials and experimental techniques

2.1. Materials and samples preparation

2.1.1. Materials

The inactive surrogate of an ILW nuclear glass (CSD-B glass), also studied by Depierre [18], was provided by the French Atomic Energy Commission (CEA) and its composition is given in Table 1 together with that of the SON68 glass (inactive surrogate of the French R7/T7 HLW glass) for comparison. The main difference is that the ILW glass is less rich in oxides simulating fission products compared to HLW, but richer in Si, Al and Na oxides.

Glass monoliths with dimensions of 25 mm × 25 mm × 0.5 mm were cut from rectangular prism, polished to 3 μm and cleaned with ethanol before use.

2.1.2. Hydration experiments

The hydration experiments were performed in stainless steel autoclaves with a Teflon liner (39 mL). The glass monolith was placed on a Teflon holder that fit into the Teflon liner [29, 35]. 8 mL of saline solution was placed underneath the holder. The autoclave was placed in a 2 cm thick aluminium container to prevent temperature gradients that may cause vapor condensation on the glass sample during the heating and cooling processes. The hydration was conducted at two temperatures, 50°C and 90°C. The relative humidity was controlled by varying the concentration of NaCl in the solution. Thus, 92% and 95% of relative humidity were respectively obtained with 13 and 6 weight % of NaCl in the solutions [36]. Two types of experiments were conducted: short-term (35 days) and long-term (365 days). A list of all the experiments can be seen in Table 2.

Table 1. Composition in weight percentage of the simulated French nuclear waste glasses SON68 and CSD-B

Oxides	SON68	CSD-B
SiO_2	45.1	50.33
B_2O_3	13.9	14.44
Al_2O_3	4.9	8.70
Na_2O	9.8	12.58
Li_2O	2.0	2.17
Cr_2O_3	0.5	0.07
CaO	4.0	3.10
Fe_2O_3	2.9	2.84
P_2O_5	0.3	0.42
ZnO	2.5	
NiO	0.4	0.33
ZrO_2		1.99
MoO_3		0.69
RuO_2		0.12
BaO		0.36
MnO_2		0.19
CoO		0.27
SO_3		0.19
Oxides (Fission Products + Zr + Actinides)	13.7	
Oxides (Fission Products + Actinides)		0.47
Other		0.74
Total	100	100

Table 2. Experimental conditions for hydration experiments. The corresponding techniques used to analyse each sample were also listed.

Relative Humidity (%)	Temperature (°C)	Alteration time (days)	Analytical techniques
92	50	365	FTIR, SEM, EDX, Micro-Raman, TEM
92	90	365	
95	50	365	
95	90	365	
92	50	35	
92	90	35	
95	50	35	
95	90	35	

Four sampling were conducted in the first month, two the following month and then one sampling every month. To do so, the autoclaves, including the overpack, were removed from

the oven and left to cool down for six hours at room temperature. Then, the glass monolith was analysed using Fourier Transform-Infrared (FTIR) spectroscopy. After the FTIR measurements, the monoliths were placed back onto the sample holder. After each sampling, the saline solution was replaced by a fresh one. No significant change of pH or of the mass of the saline solution was observed.

2.2. Characterization techniques

Glass hydration was followed using FTIR Spectroscopy. The glass monoliths, transparent to the laser beam, were analysed using a 8400 Shimadzu FTIR between 4000 and 2500 cm^{-1}. This range allowed the observance of the concentration and speciation of water in the glass [37, 38]. After spectra deconvolution, the error was estimated to 2%.

At the end of experiments, hydrated glass samples were collected from the reactor and characterised by scanning electron microscope (SEM) (JEOL JSM 5800 LV and 7600 LV, 15 kV). We carried out direct observations of the altered surface to view the crystallised secondary phases. The cross-sectional samples were prepared by polishing cross-sections of cuts perpendicular to the original surface to obtain a large-scale morphological overview, as well as to observe the chemographic relationships of the surface layers and for the thickness measurements of the glass alteration layer.

The SEM is coupled with an energy dispersive X-ray spectrometer (EDX), making quantitative chemical analysis possible on the carbon-metallised specimens. The final compositions were calculated assuming oxide stoichiometry and normalization to 100%. The EDX detected the presence of K-lines associated with Al, Si, Ca, Na, Cr, Fe, Ni and while L-lines were used for Zr and Ru. Two light elements that are important constituents of CSD-B glass, Li and B, are not detectable using this technique.

The hydrated glass was analysed using micro-Raman spectroscopy. The confocal micro-Raman was employed because it ensures a great facility of use and of its great advantages for microanalysis of mineral phases [29]. Measurements were performed at room temperature in the backscattering configuration on a T64000 Jobin-Yvon/Labraham spectrometer equipped with the diffraction grating 600 lines/mm under a microscope (Olympus Bx41) with a 100x objective focusing the 514 nm line from an Argon-Krypton ion laser. With the 100x objective, the spot size of the laser was estimated at 0.8 µm. A Peltier-

based cooled CCD records spectrum and the resolution given by the spectrometer setting is around 2 cm^{-1}. Raman measurements were carried out at very low laser power to minimize possible sample deterioration. All spectra were recorded twice in the wavenumber 100-2000 cm^{-1} region with an integration time of 360 s. We used Origin software and the gaussian curves as elementary fitting functions. The compositions of mineral phases were determined by comparing the collected Raman signals to values reported in literature. The error is estimated to 5%.

The alterated glass was also analysed using High Resolution TEM (HRTEM) with EDX and HAADF-STEM using JEOL JEM-ARM200F double Cs-corrected transmission electron microscope with the acceleration voltage of 200 kV. The FEI TIA software was used to control the STEM-EDX mapping. The best spatial resolution in STEM mode is 82 pm. The point-to-point resolution for TEM is 110 pm, in the ADF-STEM image we used, the probe size of 1 nm for obtaining better X-ray counts. EDX software controlling the acquisition of elemental map is JEOL Analysis Station 3.8. The specifications of the STEM were; CS of 1.0 mm and the probe size of 1.0 nm. The condenser aperture was 20 mm in diameter. TEM specimens were prepared by dispersing the sample on the holeycarbon thin film supported by a Cu mesh grid. For each sample, the thickness measurement of the hydrated layer was performed over several images and in different locations within the sample. Mean and standard deviation were calculated on the hydration layer thickness and the initial and long-term hydration rates. The error is 7 to 14% for the hydrated samples for 365 days and up to 27% for samples hydrated at 50 °C for 35 days.

3. Results and discussion

3.1. Infrared Results

In the work of Efimov *et al.* [39] and Navarra *et al.* [40] on the hydration of silicate glasses, it was observed the existence of the following infrared bands:

- ≈ 3595-3605 cm^{-1} attributed to OH stretching mode in SiOH.
- ≈ 3515-3518 cm^{-1} [1] attributed to OH stretching mode in the bound water silanol groups.
- ≈ 3400-3415 cm^{-1} attributed to symmetrical stretching OH mode in the fee water molecule.
- ≈ 3170-3185 cm^{-1} attributed to OH stretching mode in bound water silanol groups.
- ≈ 2700 cm^{-1} attributed to silica matrix.

To study the FTIR spectra, we performed a deconvolution with five Gaussian using the Origin 8.0 software (OriginLab). Fig. 1 shows an example of deconvolution. Note that all spectra have been normalised to their maximum and minimum intensity (I_{max} and I_{min}). We can see the quality of deconvolution obtained by the Origin 8.0 software with five Gaussian. Thus, each vibration mode can be followed.

The SiOH absorbance was used to study the glass hydration (hydrolysis) with time [25, 26, 29, 30]. The authors found a correspondance between the hydration thickness measured by SEM/TEM and the SiOH absorbance at different experimental conditions obtained by FTIR, which allowed to obtain hydration kinetics with time exposure.

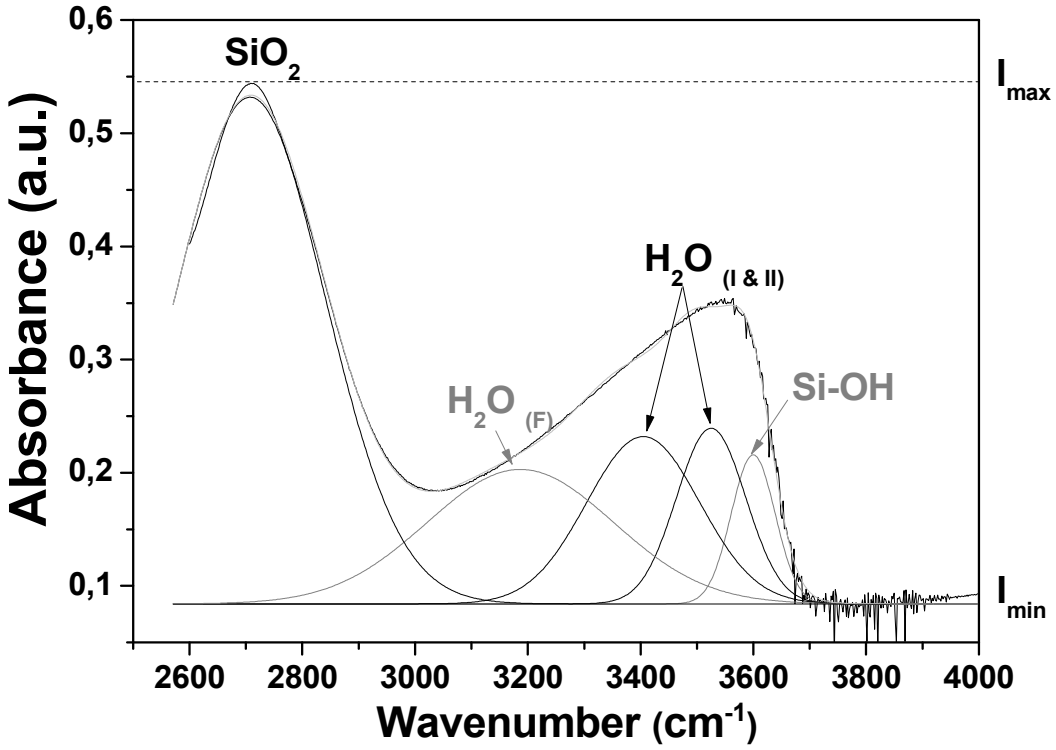

Fig. 1: Infrared spectra of CSD-B glass hydrated 1 day at 90°C under 92% of relative humidity. The spectra was deconvoluted with five gaussian.

3.1.1. Effect of relative humidity

FTIR spectra were taken for each hydrated sample and the absorbance was plotted as a function of time at 50°C and 90°C for various relative humidities. We chose to follow the evolution of the absorption band at 3595 cm^{-1} corresponding to the vibration of silanol group (SiOH), this band is indicative of the silicate hydrolysis. Fig. 2 shows the evolution of the

absorption of the silanol band as a function of hydration time at 50 °C and 90 °C, for different values of relative humidities. The absorbance values were normalised using the SiOH absorbance of the pristine glass.

At 50°C or 90°C, the initial hydration rate is linear with time. After 1 to 4 months of alteration, depending on the experimental conditions, there is a significant change in the regime with a significant drop in the hydration kinetics. This does not seem to depend on the relative humidity.

The absorbance (i.e., the hydration rate) of the SiOH band (3595 cm^{-1}) increases between 92% and 95% of relative humidity and the increase is more pronounced at 90°C. However, the effect of relative humidity is very low after the change of hydration regime and the rate seems very similar for all conditions studied here.

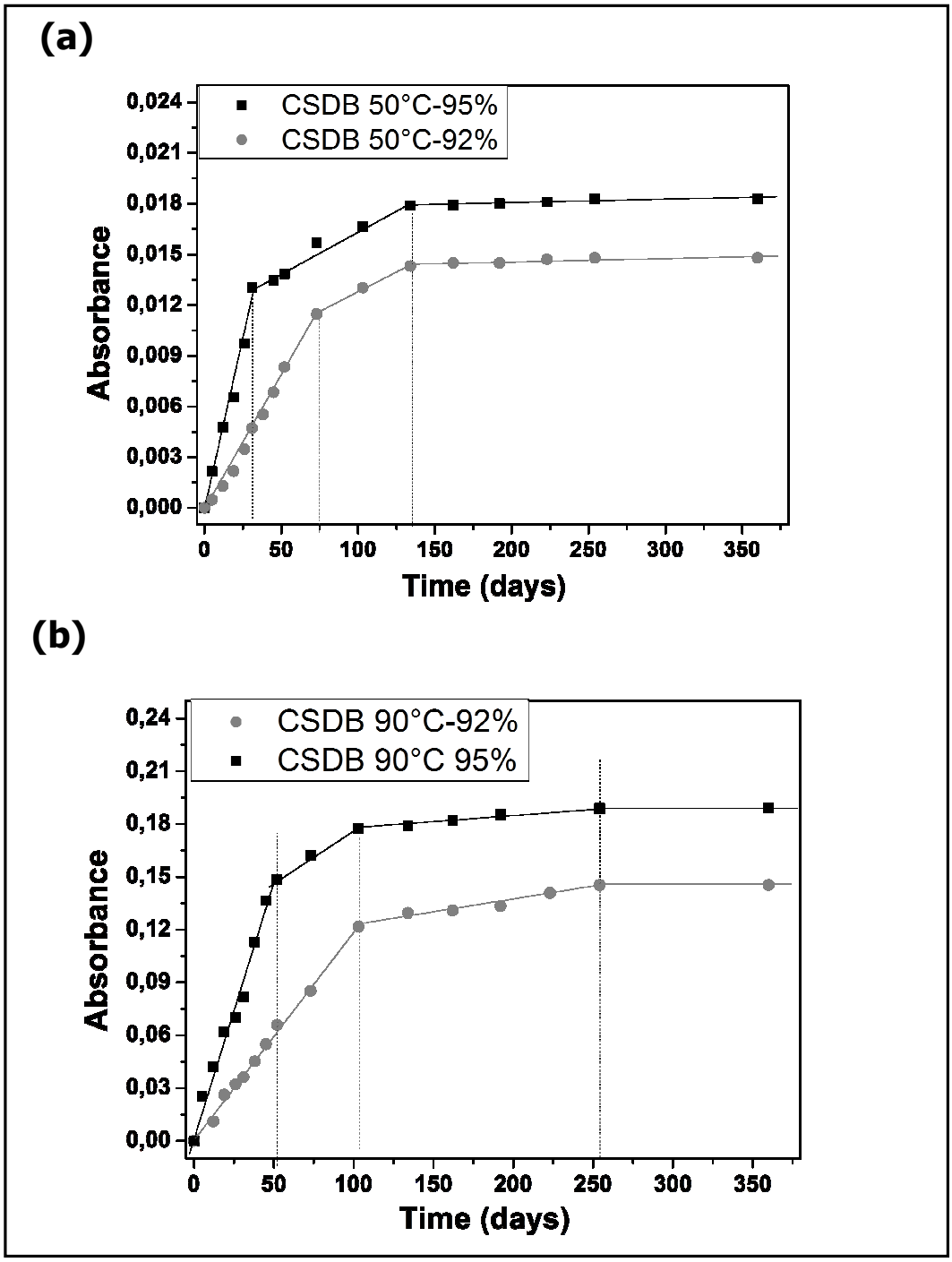

Fig. 2: Evolution with the alteration time of the absorbance (band at 3595 cm $^{-1}$ assigned to SiOH) for different relative humidity at 50 °C (a) and 90 °C (b)

3.1.2. Effect of temperature

Fig. 3 shows the absorbance relative to Si-OH band as a function of time for the CSD-B glass hydrated under 92% and 95% of relative humidity at various temperatures (50°C and 90°C). We can see a strong increase of absorbance of the Si-OH band with the temperature. An order of magnitude is noted between the alteration kinetics at 50°C and 90°C for the same relative humidity. The surface reactivity and the transfer of water through the surface layers may explain these differences.

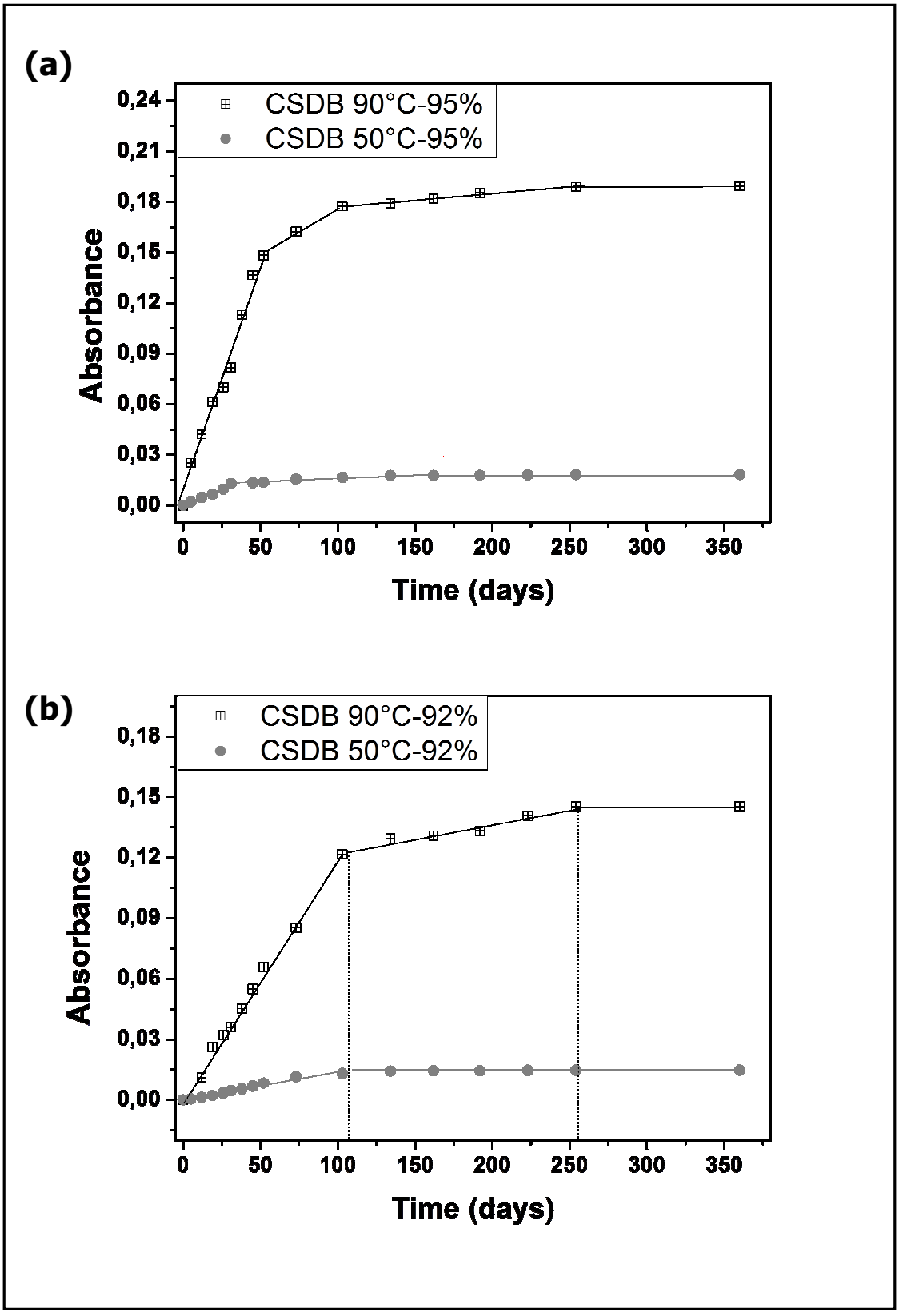

Fig. 3: Evolution with the alteration time of the absorbance (band at 3595 cm^{-1} assigned to SiOH) for different temperatures under 95% (a) and 92% (b) of relative humidity

Additional short term hydration experiments were conducted for 35 days in the same conditions in order to study the surface layer. The absorbance of the Si-OH band as a function of time are represented in Fig. 4 at 50°C and 90 °C under 92% and 95% of RH. For these short-term experiments we obtain similar absorbance units for the same hydration time compared to the long-term experiments, showing the good reproducibility of our experiments and the high accuracy of FTIR measurements.

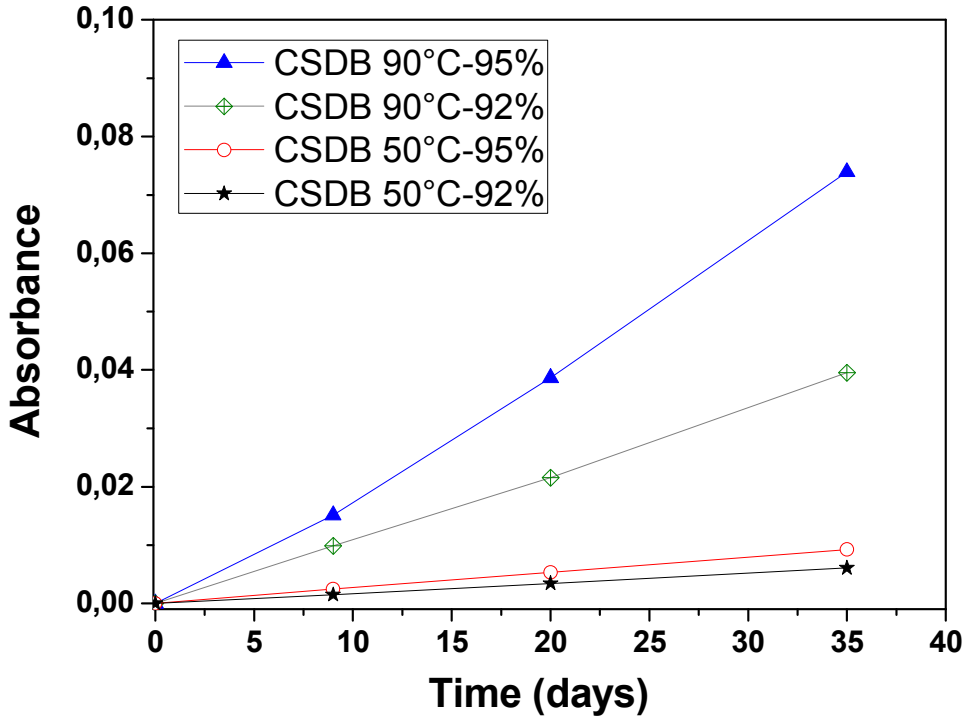

Fig. 4: Evolution with the alteration time of the absorbance (band at 3595 cm^{-1} assigned to SiOH) for the experiments conducted for 35 days at differents temperatures and relative humidities

3.1.3. Comparaison of the alteration of CSD-B and SON68 glasses

The hydration of CSD-B glass was compared to that of SON68 [41]. Fig. 5 shows the absorbance corresponding to Si-OH band as a function of time for CSD-B and SON68 glasses at 90°C under 92% and 95% of RH. As we can see, the hydration of SON68 is a little lower than CSD-B especially under 95% of relative humidity. However, this initial rate is followed by a low long-term hydration rate in both CSD-B (this work, Fig. 3) and SON68 glasses [41]. This suggests that similar hydration mechanisms are controling the long-term hydration of these two borosilicate glasses.

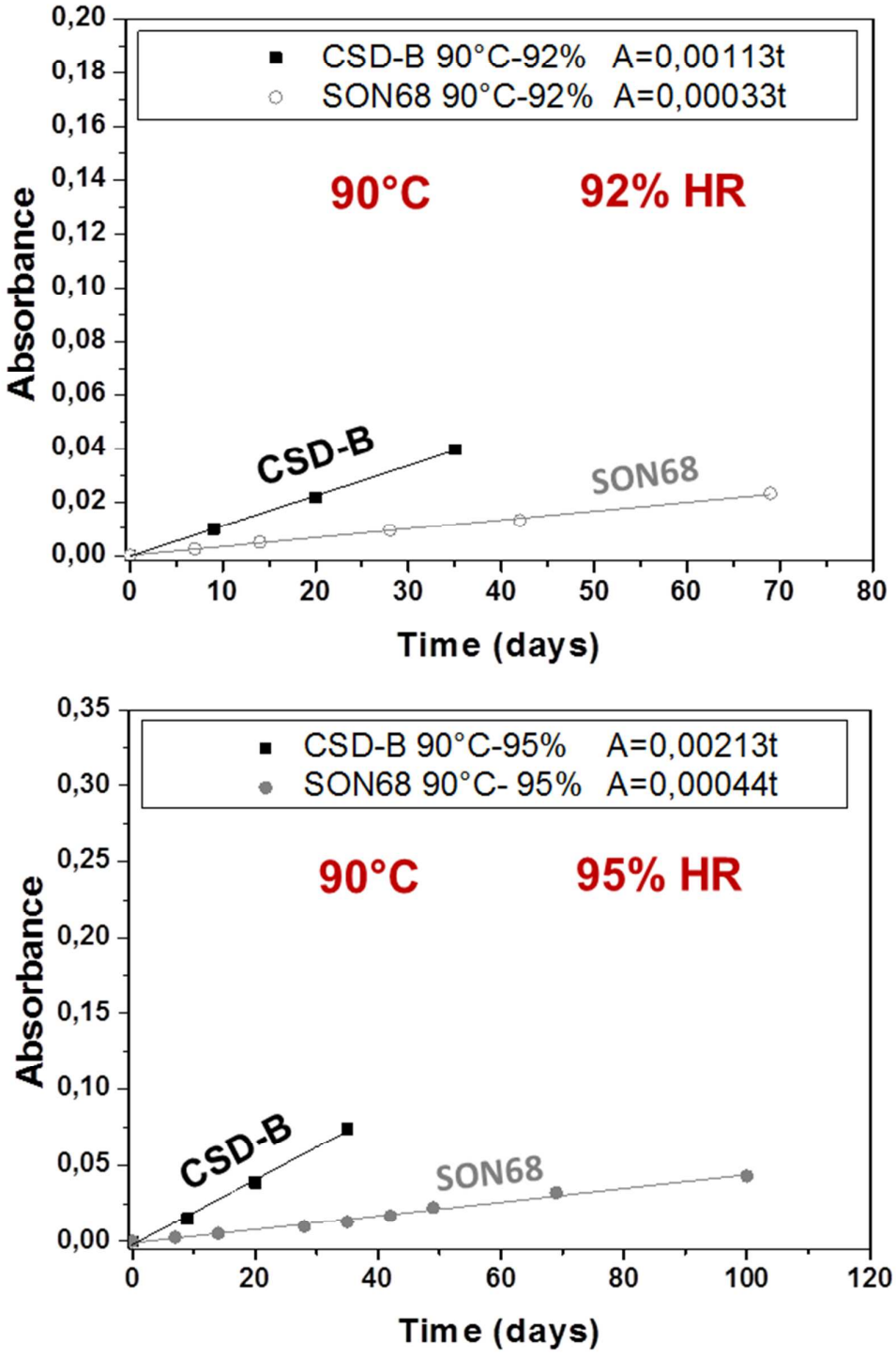

Fig. 5: Evolution with the alteration time of the absorbance (band at 3595 cm-1 assigned to SiOH) for the CSD-B and SON68 glasses at 90°C under 92% and 95% of relative humidity.

3.2. Cross sectional TEM analyses

Cross-sectional analyses of the altered glasses were performed using TEM. A typical TEM cross section, with elemental maps is given in Fig. 6 to 8 for samples hydrated for 35 and 365 days at 50 and 90°C under 92% and 95% of RH. The figures show clearly the hydration layers of a few hundred nm after 35 days to more than 1µm for samples hydrated 1 year. The Ca, Na, Si, Fe and Ni mapping and EDX analyses performed on hydrated samples show that the hydrated layer is enriched in Si and depleted in Na and Ca in comparison to the pristine glass. This elemental distribution indicates that glass components can migrate through the alteration layer perhaps via a water-saturated gel layer. The concentration of Fe and Ni is remarkably constant.

The TEM observations allowed to link the FTIR water absorbance data with the alteration layer tickness. The correspondance TEM-FTIR is deduced from the whole experimental duration For all experiments we obtained an average of 0.1 SiOH absorbance unit per 1 µm of alteration layer measured by TEM. This correspondance is close to that obtained by Neeway *et al.* [25, 26] for the SON68 glass (0.09 a.u/µm) and the value obtained by Abdelouas et al. [29] for the ISG glass (0.11 a.u/µm).

3.2.1. Short-term hydration

Fig. 6 show the TEM photographs and elemental maps (Na, Ca, Si, Fe, Ni, Zr) of glass hydrated 35 days at 90 °C under 92 and 95% of RH. The elemental maps show a depletion of Na and Ca in the hydrated layer. However, the concentrations of Fe, Zr and Ni remain unchanged compared to the pristine glass.

For the sample hydrated under 92% RH the thickness of the hydration layer is estimated to be about 205 ± 29 nm. Evidence of glass dissolution and porosity formation can be seen in Fig. 6 with a clear interface between the pristine and the hydrated glasses. The hydration rate, calculated by dividing the thickness by the glass density (2.5 g/cm^3), is $1.5\text{x}10^{-2} \pm 2.1\text{x}10^{-3}$ g/m^2.d (Table 3).

For the CSD-B glass hydrated 35 days at 90 °C and 95 % of RH, the thickness of the altered layer is estimated to about 225 ± 24 nm, giving a hydration rate of $1.6\text{x}10^{-2} \pm 1.7\text{x}10^{-3}$ g/m^2.d. (Table 3). This rate is in the same order of magnitude as that calculated at 90 °C and 92 % of RH and is similar to that found by Bouakkaz *et al.* [41] for the SON68 glass hydrated in the same conditions (1.20×10^{-2} g/m^2.d).

The determination of the hydrated layer thickness at 50 °C for the short term experiments (35 days) is delicate because it is very thin and the chemical contrast between pristine and hydrated glass layer is very low. Nevertheless, we were able to estimate the hydration layer to about 80 ± 21 nm at 50°C and 95% of RH. This corresponds to an initial hydration rate of $5.7x10^{-3} \pm 1.5x10^{-3}$ g/m^2.d (Table 3). This rate is 3 times lower than that calculated at 90 °C for the same relative humidity. For the glass hydrated at 50°C and 92% of RH, the hydrated layer is estimated to 65 ± 21 nm, which corresponds to the alteration rate of $4.6x10^{-3} \pm 1.5x10^{-3}$ g/m^2.d (Table 3).

Table 3: The thickness of the reaction layer given by TEM and FTIR. The TEM value was obtained from cross sections. The FTIR values were calculated using the correspondance TEM – FTIR (0.1 a.u/µm) based on TEM observations for samples hydrated for 365 days

	TEM		FTIR	
Sample	Layer thickness (nm)	r_{hydr0} (g/m^2.d.)	Layer thickness (nm)	r_{hydr0} (g/m^2.d.)
90°C, 92% RH, 35 days	205 ± 29	$1.5x10^{-2} \pm 2.1x10^{-3}$	333 ± 7	$2.8x10^{-2} \pm 5.6x10^{-4}$
90°C, 95% RH, 35 days	225 ± 24	$1.6x10^{-2} \pm 1.7x10^{-3}$	625 ± 13	$4.4x10^{-2} \pm 8.8x10^{-4}$
50°C, 92% RH, 35 days	65 ± 21	$4.6x10^{-3} \pm 1.5x10^{-3}$	51 ± 1	$4.3x10^{-3} \pm 8.6x10^{-5}$
50°C, 95% RH, 35 days	80 ± 21	$5.7x10^{-3} \pm 1.5x10^{-3}$	77 ± 2	$7.1x10^{-3} \pm 1.4x10^{-4}$

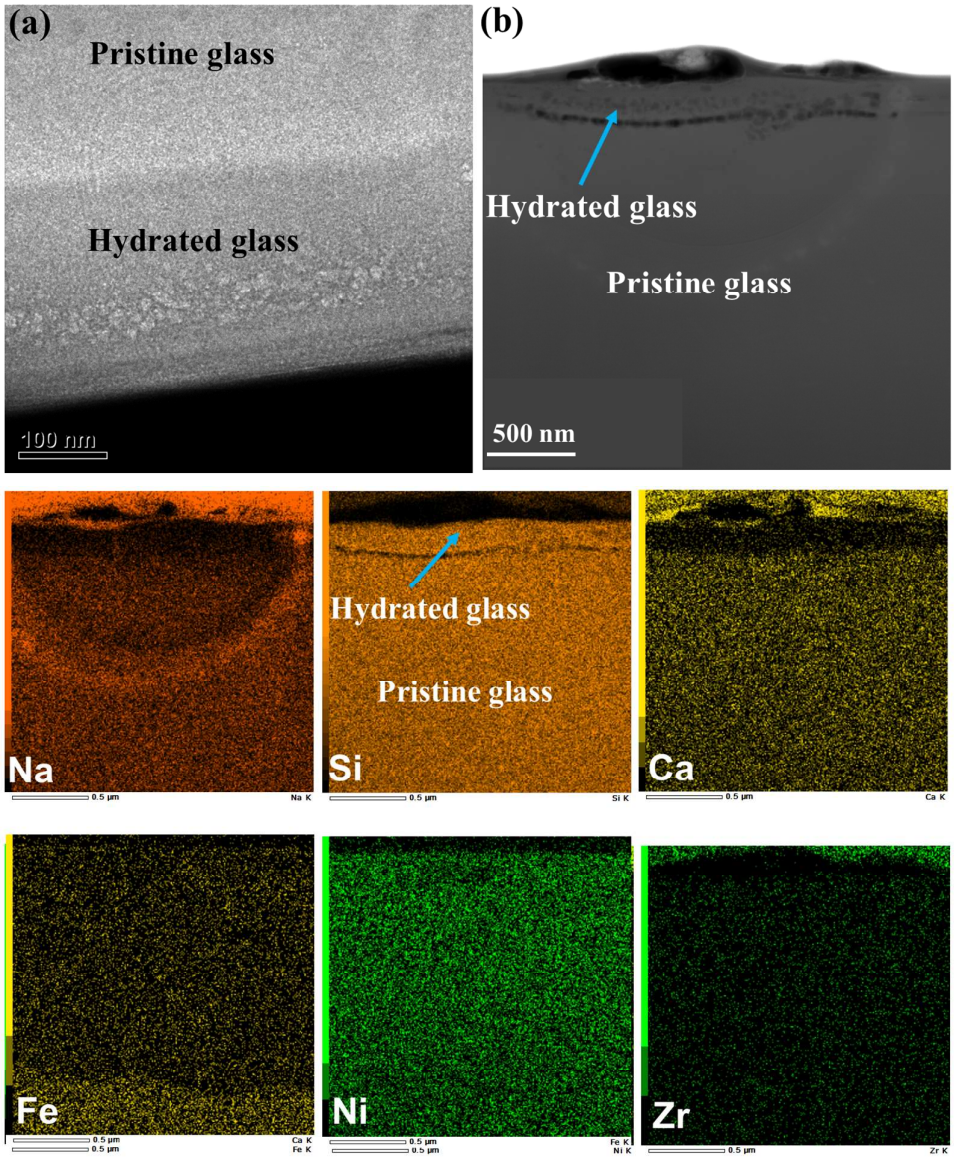

Fig. 6: TEM photographs of CSD-B glass hydrated 35 days at 90°C and (a) 95% and (b) 92% of RH. The Na, Si, Ca, Fe, Ni and Zr maps of the sample hydrated 35 days at 90°C and 92% RH are also represented.

3.2.2. Long-term hydration

TEM observations show a highly porous hydration layer with a hydration front, showing strong dissolution evidence at the interface glass/hydration layer. Elemental mapping confirms a strong loss of Na and Ca while heavy elements such as Fe and Ni remain unchanged.

The results of TEM thickness measurements for long-term experiments could not directly be used to calculate a long-term hydration rate because the total thickness also includes that

corresponding to the short-term rate. However, the long term hydration rate, corresponding to the period starting from the second inflection of the glass hydration until the end of the experiment, was calculated from the FTIR data (Fig. 2 and 3) and using the correspondence TEM – FTIR (0.1 a.u/µm) (Table 4). The long-term rate is in the order of 10^{-3} g/m^2.d at 90°C and $5.0\text{x}10^{-5}$ g/m^2.d at 50°C. These rates are one order of magnitude lower than the initial rates and in the same order of magnitude than that found for the SON68 glass [25, 41]. For example for the sample hydrated at 90°C and 95% of RH, we found a long-term rate of $1.2\text{x}10^{-3} \pm 2.3\text{x}10^{-5}$ g/m^2.d for the CSD-B glass compared to 1.6×10^{-3} g/m^2.d for the SON68 glass [41]. Table 5 summarizes the short and long-term hydration rates of CSD-B and SON68 glasses and indicates the similarity between these two glasses.

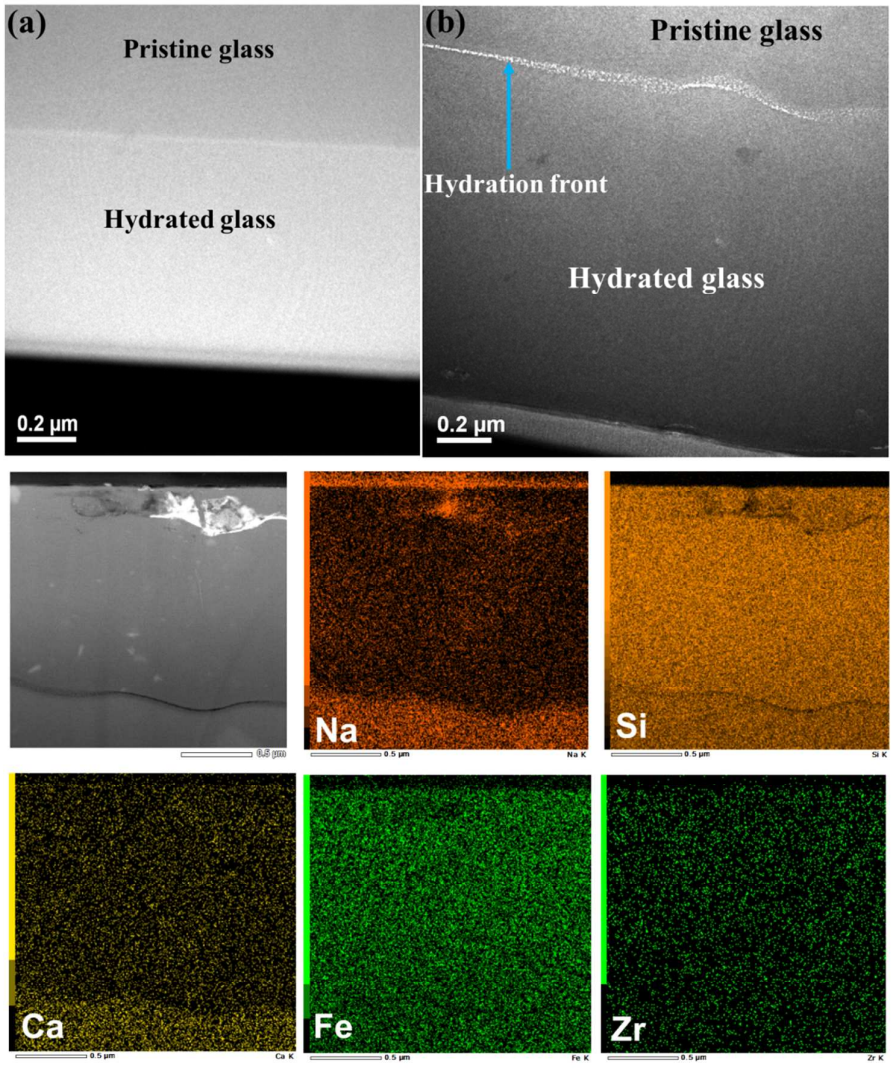

Fig. 7: TEM photographs of CSD-B glass hydrated 365 days at 90°C and (a) 92% and (b) 95% of RH. The Na, Si, Ca, Fe and Zr maps of the sample hydrated 365 days at 90°C and 95% of RH are also represented.

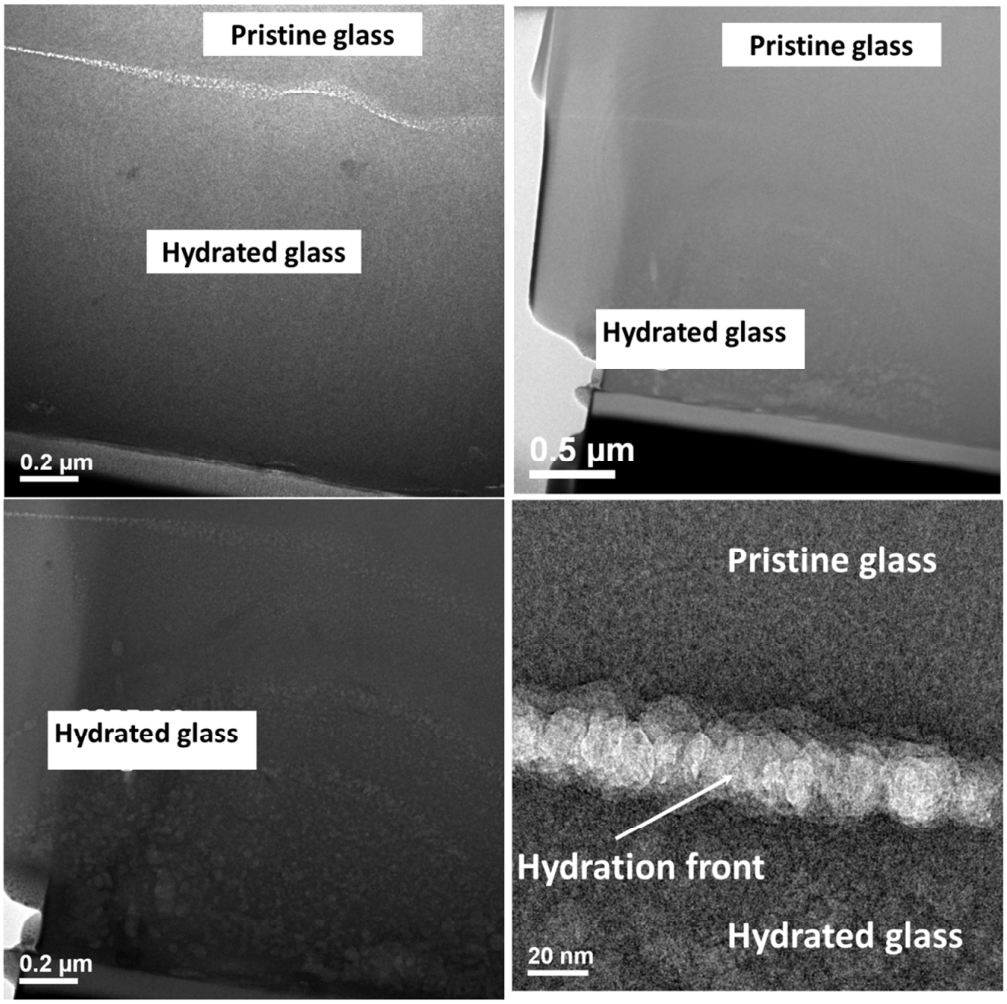

Fig. 8: TEM photographs of CSD-B glass hydrated 365 days at 90°C and 95% of RH.

Table 4: The long-term reaction rate calculated from FTIR absorbance using the correspondence TEM – FTIR (0.1 a.u/µm).* the data correspond to the period starting from the inflection of the glass hydration until the end of the experiment.

Sample	long-term calculated layer thickness (nm)*	$r_{hydr\ L.T}$ ($g/m^2.d.$)	Total layer thickness by TEM (nm)
90°C, 92% RH, 365 days	237 within the last 267 days	$2.3x10^{-3} \pm 4.6x10^{-5}$	695 ± 75
90°C, 95% RH, 365 days	119 within the last 267 days	$1.2x10^{-3} \pm 2.3x10^{-5}$	1500 ± 104
50°C, 92% RH, 365 days	5 within the last 226 days	$5.5x10^{-5} \pm 1.1x10^{-6}$	150 ± 22
50°C, 95% RH, 365 days	4 within the last 226 days	$4.4x10^{-5} \pm 8.8x10^{-7}$	270 ± 23

Table 5: The initial and long-term hydration rate of the CSD-B and SON68 glasses

Sample	CSD-B		SON68 [41]	
	r_{hydr0} (g/m^2.d.)	$r_{hydr\ L.T}$ (g/m^2.d.)	r_{hydr0} (g/m^2.d.)	$r_{hydr\ L.T}$ (g/m^2.d.)
90°C, 92% RH	$1.5x10^{-2} \pm 2.1x10^{-3}$	$2.3x10^{-3} \pm 4.6x10^{-5}$	$9.8x10^{-3}$	$2.3x10^{-3}$
90°C, 95% RH	$1.6x10^{-2} \pm 1.7x10^{-3}$	$1.2x10^{-3} \pm 2.3x10^{-5}$	$1.2x10^{-2}$	$1.6x10^{-3}$
50°C, 92% RH	$4.6x10^{-3} \pm 1.5x10^{-3}$	$5.5x10^{-5} \pm 1.1x10^{-6}$	$5.2x10^{-3}$	$9.2x10^{-4}$

3.3. SEM imaging and EDX analyses

The CSD-B glass hydrated 35 days and 365 days was observed by SEM and analysed by EDX after carbon metallisation. To check the sensitivity of EDX, we analysed the pristine glass and the analysed composition is compared to the theoretical composition in Table 1. The measured composition is in good agreement with the initial glass composition and shows the high sensitivity of the used device. Note that the measured composition is normalised to 83.39% to take into account the boron and lithium percentage unmeasured by EDX.

Fig. 9a and 9b shows the SEM photograph and EDX spectra of CSD-B glass hydrated for the short term (35 days) at 50°C and 90°C under 92% and 95% of RH. The EDX microanalyses in Table 6 show no significant difference between the composition of the hydrated and pristine glass. This is probably due to the small thickness of the hydrated layers for all experiments (65-225 nm), which is largely less than the analysed thickness (1 µm). We can notice the presence of dissolution evidence on the glass surface in all experiments.

Table 6: EDX microanalysis of the surface of the CSD-B glass hydrated 35 days at 50°C and 90°C and 92% and 95% RH. The data correspond to an average of 6 spot analyses.

Oxides	**Pritine glass**	**92 % RH, 50°C, 35 d**	**95 % RH, 50°C, 35 d**	**92 % RH, 90°C, 35 d**	**95 % RH, 90°C, 35 d**
SiO_2	63.6 ± 0.61	65.2 ± 0.41	63.3 ± 0.10	64.2 ± 0.14	66.4 ± 0.04
Al_2O_3	10.7 ± 0.22	11.0 ± 0.10	10.7 ± 0.03	10.5 ± 0.09	10.8 ± 0.06
Na_2O	12.3 ± 0.19	12.0 ± 0.30	11.6 ± 0.03	12.4 ± 0.21	10.8 ± 0.28
Cr_2O_3	0.3 ± 0.19	0.4 ± 0.03	0.4 ± 0.04	0.0 ± 0.05	0.5 ± 0.03
CaO	3.8 ± 0.16	3.8 ± 0.05	3.9 ± 0.04	3.3 ± 0.07	3.5 ± 0.06
Fe_2O_3	3.2 ± 0.15	3.1 ± 0.08	3.3 ± 0.11	3.3 ± 0.06	3.2 ± 0.04
P_2O_5	0.4 ± 0.26	0.4 ± 0.03	0.3 ± 0.04	0.4 ± 0.05	0.5 ± 0.06
NiO	0.3 ± 0.22	0.3 ± 0.04	0.3 ± 0.02	0.5 ± 0.06	0.3 ± 0.04
ZrO_2	3.2 ± 0.17	3.5 ± 0.11	3.6 ± 0.09	3.3 ± 0.20	3.1 ± 0.23
La_2O_3	0.2 ± 0.12	0.0 ± 0.0	0.0 ± 0.0	0.0 ± 0.0	0.0 ± 0.0

Ce_2O_3	1.2 ± 0.11	1.2 ± 0.10	1.2 ± 0.10	1.2 ± 0.14	1.1 ± 0.13
Nd_2O_3	0.7 ± 0.34	0.7 ± 0.07	0.7 ± 0.03	0.5 ± 0.08	0.7 ± 0.11
RuO_2	0.0 ± 0.0	0.0 ± 0.0	0.0 ± 0.0	0.0 ± 0.0	0.0 ± 0.0
Total	100	100	100	100	100

Fig. 9 shows the SEM photographs of CSD-B glass hydrated 365 days at 50°C and 90°C under 92% and 95% of RH. The SEM photographs show alteration layers consisting of a gel-like layer with cracks. The formation of gel is more advanced for higher temperatures (90°C) and RH (95%). However, there is no significant difference between 92% and 95% RH. We also see the formation of ruthenium particles (Fig. 9) in the case of experiments conducted at 90°C. The RH had no effect on layer composition while the temperature influenced the gel composition (Table 7). Hence, the gel composition shows the loss of Na and Ca compared to the pristine glass. These results are in good agreement with TEM data. The concentration of ZrO_2 and Fe_2O_3 is remarkably constant in all samples regardless of temperature and RH underlying the low mobility of these elements often observed during the aqueous corrosion of nuclear glasses [25, 26].

At 50°C, the EDX analyses of hydrated glass are similar to those of the pristine glass, regadless of the RH, which is attributed to the small tickness of the gel layer at 50°C (150 to 270 nm), which is largley below the analysed depth (1 μm).

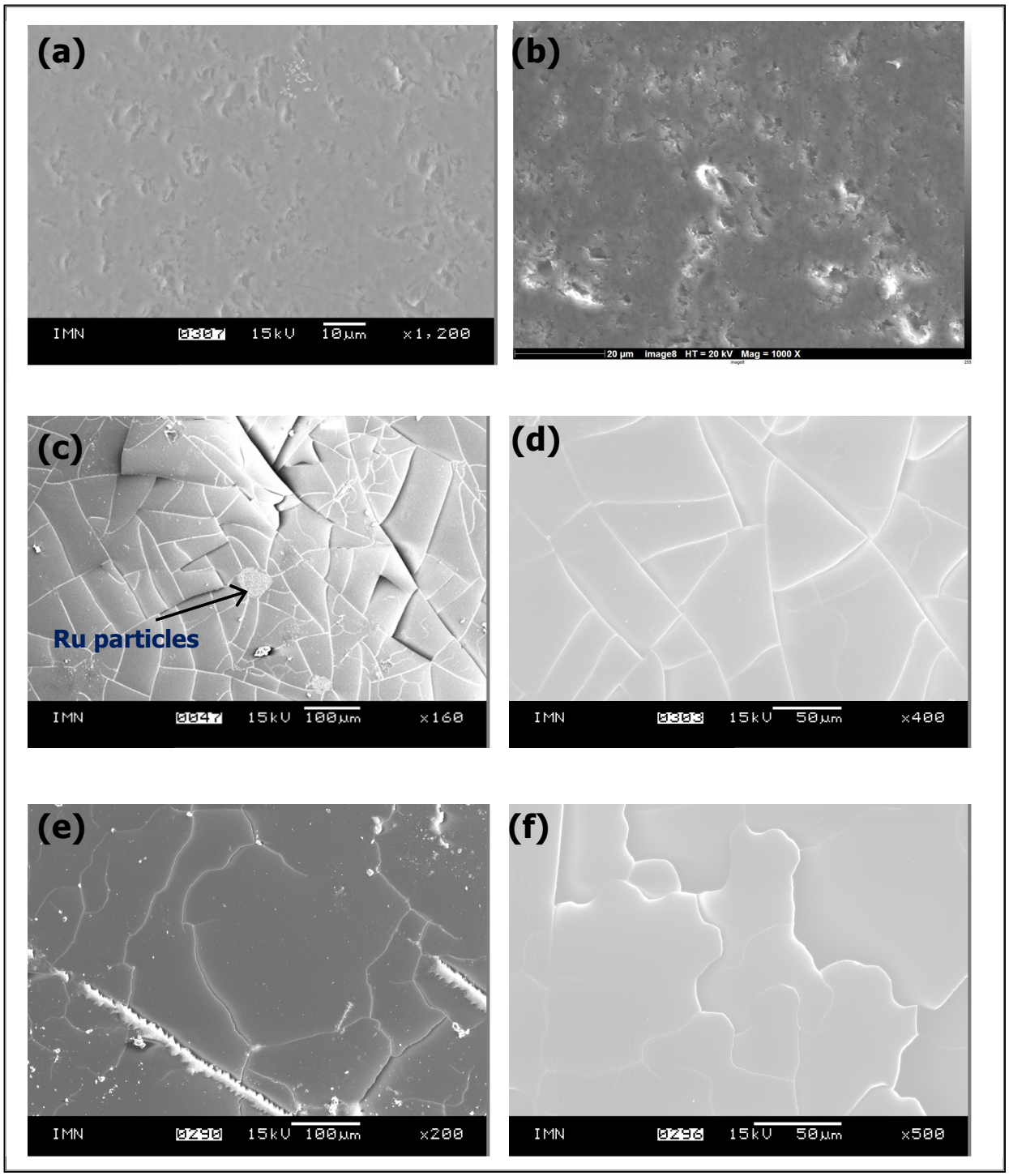

Fig. 9: SEM photograph of the surface of altered CSD-B glass, (a):35 days at 90°C and 92% RH, (b):35 days at 50°C and 95% RH, (c):365 days at 90°C and 92% RH, (d):365 days at 90°C and 95% RH showing the gel formation and Ru particles, (e): 365 days at 50°C and 95% RH, (f): 365 days at 50°C and 92% RH

Table 7: EDX microanalysis of the surface of the CSD-B glass hydrated at 50°C and 90°C for 365 days and a relative humidity of 92% and 95%. The data correspond to an average of 6 spot analyses.

Oxides	Pristine glasss	92 % RH, 50°C, 365 d	95 % RH, 50°C, 365 d	92 % RH, 90°C, 365 d	95 % RH, 90°C, 365 d
SiO_2	63.6 ± 0.61	63.2 ± 0.95	63.0 ± 0.72	67.9 ± 0.62	69.9 ± 0.92
Al_2O_3	10.7 ± 0.22	10.4 ± 0.05	10.5 ± 0.07	12.8 ± 0.08	11.8 ± 0.11
Na_2O	12.3 ± 0.19	13.9 ± 0.53	13.0 ± 0.61	6.8 ± 0.45	6.5 ± 0.35
Cr_2O_3	0.3 ± 0.19	0.1 ± 0.09	0.4 ± 0.07	0.3 ± 0.08	0.2 ± 0.06
CaO	3.8 ± 0.16	3.2 ± 0.41	3.4 ± 0.52	1.5 ± 0.33	1.3 ± 0.43
Fe_2O_3	3.2 ± 0.15	3.1 ± 0.16	3.5 ± 0.20	3.9 ± 0.19	3.9 ± 0.13
P_2O_5	0.4 ± 0.26	0.7 ± 0.12	0.2 ± 0.14	0.7 ± 0.21	0.8 ± 0.15
NiO	0.3 ± 0.22	0.5 ± 0.10	0.2 ± 0.09	0.5 ± 0.08	0.4 ± 0.11
ZrO_2	3.2 ± 0.17	2.3 ± 0.05	3.1 ± 0.08	3.0 ± 0.07	2.9 ± 0.06
La_2O_3	0.2 ± 0.12	0.3 ± 0.09	0.0 ± 0.0	0.1 ± 0.08	0.1 ± 0.07
Ce_2O_3	1.2 ± 0.11	1.4 ± 0.13	1.1 ± 0.11	1.3 ± 0.09	1.2 ± 0.10
Nd_2O_3	0.7 ± 0.34	0.6 ± 0.08	0.9 ± 0.07	0.9 ± 0.08	0.8 ± 0.11
RuO_2	0.0 ± 0.0	0.1 ± 0.03	0.3 ± 0.05	0.1 ± 0.07	0.0 ± 0.0
Total	100	100	100	100	100

3.4. Micro-Raman analyses

The Raman spectroscopy of borosilicate glasses is one of the non-destructive tool to determine the glass structure. The Raman analysis may be successfully applied to a large variety of glass as encountered in the field of craft history and archaeology. The structure of the silicate network in a glass is mainly determined by the degree of polymerization of the silicate tetrahedra and described by the abundance of different Q_n species, where Q_n denotes a tetrahedron linked by bridging O atoms to n adjacent tetrahedra. The range of n is 0 (isolated tetrahedra) to 4 (fully polymerized three-dimensional network). Therfore, the analyses of the stretching band of Si-O bond species Q_n in silicate glasses envelope of a given silicate can then provide useful information about its microstructure. It was proposed by Colomban [42,43] that the relative intensities of the bending and stretching bands can provide good indication of the degree of polymerization of a silicate because of modification of the partial charge of oxygen atoms involved in the Si-O bonds [44].

The Raman vibration modes present in this type of glass were widely studied. We will report those present in the litterature:

- The broad band around 490 cm^{-1} is assigned to the stretching modes of Si-O-Si [45-47].

- The centered peak at 680 cm^{-1} is attributed to vibrations involving type rings danburite B_2O_7-Si_2O_7 [48, 49].

- The broad band between 850 and 1200 cm^{-1} is associated with the symmetric stretching modes of Si-O bond species Q_n in silicate glasses. Q_n species are defined as consisting of SiO_4 tetrahedra n bridging oxygens:

• The Q_0 species are centered at 870 cm^{-1}

• The Q_1 species are centered at 900 cm^{-1}

• The Q_2 species are located at 950-1100 cm^{-1}

• The Q_3 species are located at1050 to 1100 cm^{-1}

• The Q_4 species are located at 1100-1200 cm^{-1}

- The broad band centered around 1430-1450 cm^{-1} is assigned to the stretching vibration modes of BO-binding [50-56].

The CSD-B pristine glass

Fig. 10 show the spectrum of CSD-B pristine glass. The refinement of the Raman spectrum was possible with 9 Gaussian. The Table 8 present the refined values.

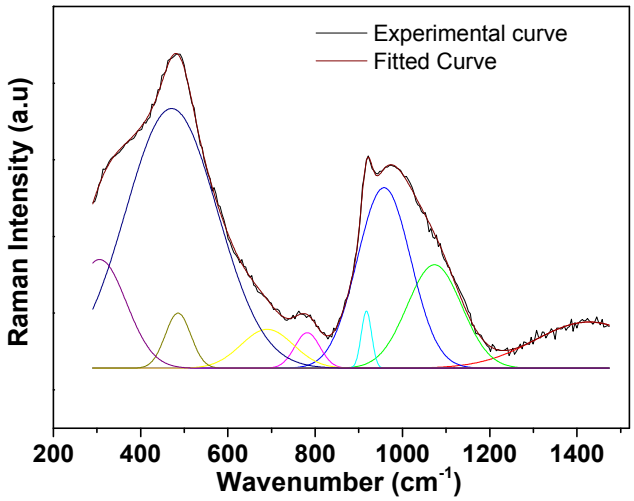

Fig. 10 Raman spectrum of the CSD-B glass reference. Example of Raman spectrum deconvolution of with 9 Gaussian.

Table 8: Refined parameters for Gaussian functions calculated for the Raman spectrum of pristine CSD-B glass.

Peaks	Vibration mode	Center	%
1	BO-binding	1427	9.2
2	Q_3	1085	10.2
3	Q_2	965	17.6
4	Q_1	917	1.1
5	Si–O stretching	785	1.6
6	Danburite B_2O_7-Si_2O_7	690	3.7
7	Si-O-Si stretching	488	2.5
8	O—(Al, Si)—O bending	475	43.4
9	Ca-O polyhedra	318	10.6
Total	-	-	100

The CSD-B glass is composed of several oxides, that does not make easy the detailed analysis and direct attribution of vibration bands. However, we can show the presence of broad bands corresponding to the vibration modes of the Q_1, Q_2 and Q_3, species localized at 917, 965 and 1085 cm^{-1}). The vibration mode at 318 cm^{-1} was attributed to the Raman vibrations involving Ca-O polyhedra [57]. The broad band at 488 cm^{-1} is assigned to the vibration modes of twisting

and stretching of the Si-O-Si [45-47]. Other bands contributions were present in the spectrum, such as the vibration mode at 690 cm^{-1} attributed to a poorly crystalline calcium silicate [58,59]. The broad band centered around 1427 cm^{-1} is assigned to the stretching vibration modes of BO-binding. The spectra are dominated by the bending modes at 475 cm^{-1} witch correspond to O—(Al, Si)—O bending. [46,47]. The band at 785 cm^{-1} is assigned to Si–O stretching vibration with a dominant Si motion [60].

The CSD-B glass after hydration

In the first time we analyzed the structural properties of CSD-B glass before (CSD-B pristine glass) and after hydration (CSD-B gel glass).

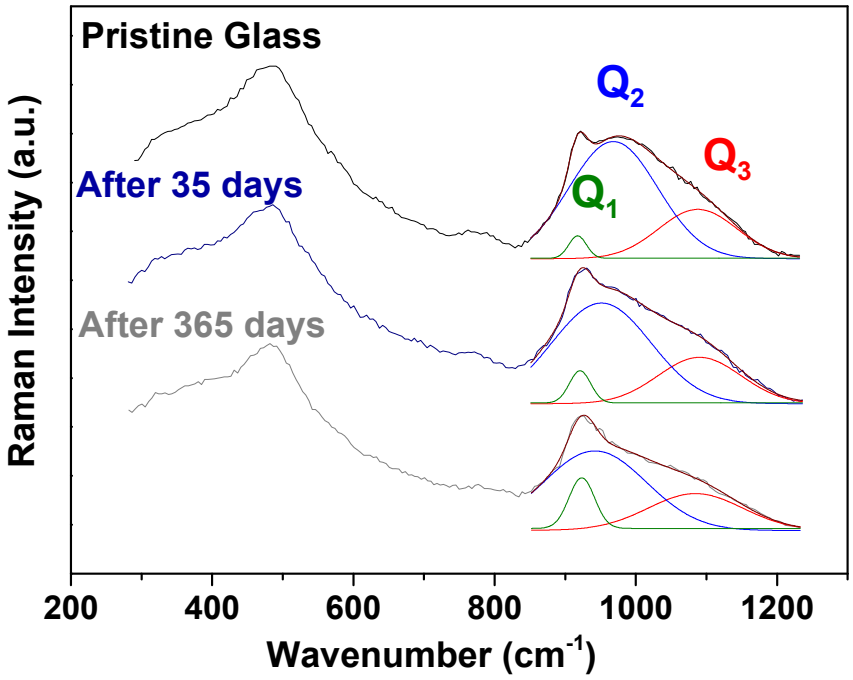

Fig. 11: Raman spectrum of the CSD-B glass before and after hydration (90 °C and 95 % of RH). The symmetric stretching modes of Si-O bond species Q_n in CSD-B glasses before and after hydration.

Table 9: Refined parameters for Gaussian functions calculated for the symmetric stretching modes of Si-O bond species Q_n in CSD-B glass.

Peaks	Vibration mode	Peak center	% of Qn peaks in the gel layer		
			Pristine glass	After 35 days	After 365 days
1	Q_3	1080-1090	35.3	32.3	23.8
2	Q_2	950-965	60.9	56.6	53.9
3	Q_1	917-923	3.8	11.1	22.3
Total	-	-	100	100	100

The Raman spectra of CSD-B glass before and after hydration (35 and 365 days are presented in Fig. 11 and Table 9 presents the refined values obtained for the stretching band of Si-O bond species Q_n in our silicate glasses. The Raman spetrum of pristine glass shows that the vibrations of the edge groups in structural units Q_3 and Q_2 are dominant in the CSD-B glasses.

With increasing the vapor hydration time, the abundance of Q_3 and Q_2 units in the glass clearly decreases (Table 9). The structure of the glass is thus depolymerized, presumably by formation of Si-OH groups from bridging O atoms according to the equation:

$$Si - O - Si + H_2O \rightarrow Si - OH + HO - Si$$

The formation of Si-OH groups has been associated with the increase of a Q_1 species peak around 920 cm^{-1} at the expense of Q_3 and Q_2 in hydrous silicate glasses. This suggests that water reacts with O atoms bridging two Q_3 tetrahedra according to $Q_3 - Q_3 \rightarrow Q_2 - Q_2 \rightarrow Q_1 - Q_1$.

The minerals formed on the CSD-B gel glass surface

Raman spectra of the mineral phases formed after 35 and 365 days on CSD-B glass monolith surface are shown in Fig. 12. The only mineral phases detected with Raman spectroscopy are a few particles of calcite ($CaCO_3$), apatite $Ca_5(PO_4)_3(OH)$ and elemental Ru.

The Raman spectrum of apatite is dominated by the stretching vibration of the P–O bonds. The band at around 962 cm^{-1} corresponds to the symmetric stretching vibration (ν_1) of phosphate (PO_4^{3-}) and is the strongest marker of apatite. The spectra displayed other Raman PO_4^{3-} vibration bands such as the ν_2 symmetrical bending centred at 433 cm^{-1}, ν_4 symmetrical bending centred at 590 cm^{-1}, and ν_3 asymmetrical stretching mode centred at 1044 cm^{-1}. The

peak at 1073 cm^{-1} was formed by the carbonate (CO_3^{2-}) vibrational mode and indicated the extent of carbonate incorporated into the apatite lattice. The 1070 cm^{-1} band historically has been assigned to the A_{1g} mode of carbonate [61–65]. Recently, however, Antonakos et al. [66], Mason et al. [67], and Brooker et al. [68] have suggested that this carbonate-induced band is an asymmetric ν_3 phosphate stretch.

For calcite, there are basically five Raman bands at ambient conditions. The most intense band is the A_{1g} mode at 1085 cm^{-1} [69,70]. Two sets of doubly degenerate internal E_g modes are observed at 712 and 1434 cm^{-1}, and the external E_g or lattice modes occur at 282 and, 156 cm^{-1}. The external modes are associated with librations of the carbonate ions in the primitive cell around axes normal to the C_3 axis and translations of the CO_3^{2-} ions normal to the C_3 axis, respectively. The precipitation of carbonate minerals in these systems can affect the physical properties of the subsurface such as porosity and permeability.

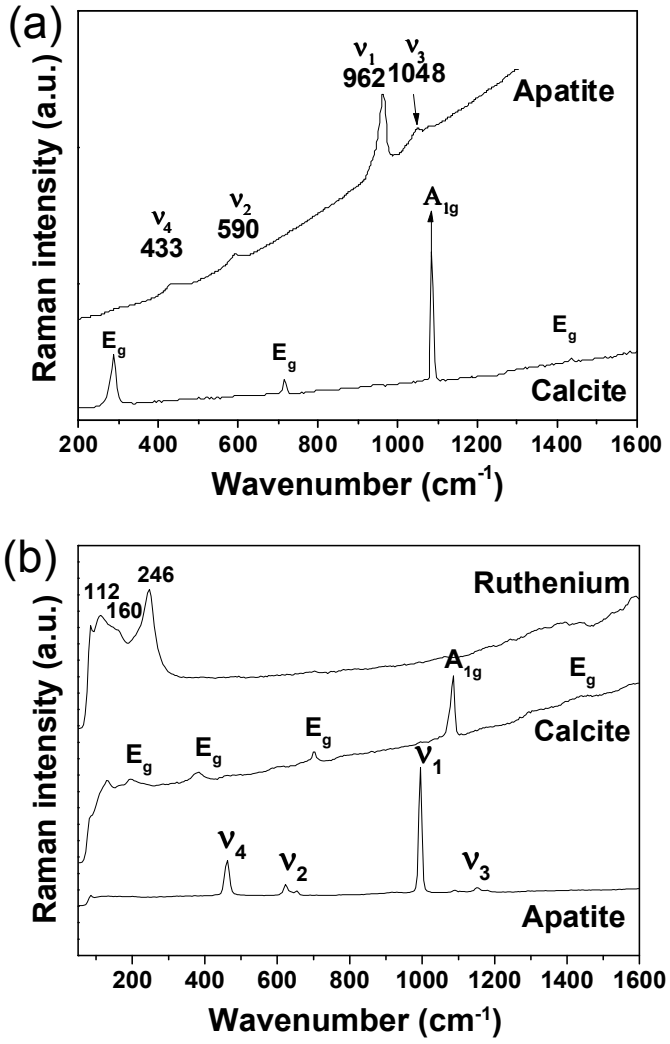

Fig. 12: Raman spectra of the precipitated products formed on CSD-B glass monolith hydrated at 90°C and 95 % of RH (a) after 35 days and (b) after 365 days.

Raman spectrum of the minerals formed on CSD-B glass monolith after 365 days is shown in Fig. 12-b. The Raman spectrum shows the precipitation of elemental Ru particles as we have seen by SEM/EDS analysis. The spectral features at low-frequency region (<300 cm^{-1}) are very similar to those reported by Slebodnick et al. [71] who attributed the vibrations modes at low-frequency to Ru-Ru stretching deformation. It's important to notice that apatite and calcite are also present on the surface of CSD-B glass after 365 days of hydration.

4. Conclusions

The borosilicate CSD-B glass vapor hydration has been studied at 50 and 90°C, and 92% and 95% relative humidities (RH) for up to one year. The glass hydration increased with temperature and RH. After a few weeks with a linear initial rate (~2×10^{-2} g/m^2.d at 90°C and ~5×10^{-3} g/m^2.d at 50°C) a drastic drop in hydration rate occurred in all experiments where the rate did not change between 255 and 365 days. The kinetic data are similar to those obtained with the French reference high-level nuclear waste glass SON68. The major hydration product is a depolymerized gel layer depleted in Na and Ca in addition to a few particles of calcite and apatite precipitated on the glass surface. Future work should focus on understanding of the mechanisms responsible for the hydration process (initial rate, final rate) and the chemical balance of leachable elements including Ca and Na to better simulate the glass behaviour under long-term disposal conditions in particular under non-saturated water conditions.

Acknowledgements

The authors acknowledge Andra for the financial support, CEA and Areva NC for the supply of ILW glass samples. Special thanks to Nicolas Stephant and Eric Gautron from Institut des Matériaux de Nantes (IMN) for SEM and TEM analyses.

References

1 D. E. Clark, C. G. Pantano Jr. and L. L. Hench, Corrosion of Glass, New York, Magazines for Industry, 1979.

2 R. G. Newton, Glass Technology, 1985, 26, 21.

3 B. C. Bunker, Mater. Res. Soc. Symp. Proc., 1987, 84, 493.

4 D. E. Clark, R. L. Schulz, G. G. Wicks and A. R. Lodding, Mater. Res. Soc. Symp. Proc., 1994, 333, 107.

5 W. H. Casey and B. C. Bunker, Mineralogical Society of America, 1990, 23, 397.

6 G. Leturcq, G. Berger, T. Advocat and E. Vernaz, Chem. Geol., 1999, 160, 39.

7 P. Jollivet, P. Frugier, G. Parisot, J. P. Mestre, E. Brackx, S. Gin and S. Schumacher, Journal of Nuclear Materials, 2012, 420 (1–3), 508.

8 P. Jollivet, S. Gin and S. Schumacher, Chemical Geology, 2012, 330–331, 207-217

9 P. Aagard and H. C. Helgeson, American Journal of Science, 1982, 282, 237.

10 B. Grambow, Mater. Res. Soc. Symp. Proc., 1985, 44, 15.

11 T. Advocat, Ph.D thesis, University Louis Pasteur of Strasbourg, 1991.

12 C. Jégou, Ph.D thesis, University of Montpellier II, 1998.

13 Y. Linard , Ph.D thesis, University Denis Diderot, 2000.

14 S. Gin, Mater. Res. Soc. Symp. Proc., 2001, 663, 207.

15 G. Berger, C. Claparols, C. Guy, V. Daux, Geochim. Cosmochim. Acta, 1994, 58 (22), 4875.

16 N. Valle, Ph.D thesis, Institut National Polytechnique de Lorraine, 2000.

17 S. Gin and J.-P. Mestre, Journal of Nuclear Materials, 2001, 295, 83.

18 S. Depierre, Ph.D Thesis, University of Montpellier, 2012.

19 S. Mercado-Depierre, F. Angeli, F. Frizon and S. Gin, Journal of Nuclear Materials, 2013, 441 (1–3), 402.

20 F. Bellmann, T. Sowoidnich, H. M. Ludwig and D. Damidot, Cem. Concr. Res., 2012, 42, 1189.

21 S. Gin, J. V. Ryan, D. K. Schreiber, J. Neeway and M. Cabié, Chem. Geol., 2013, 349–350, 99–109.

22 S. Garrault-Gauffinet and A. Nonat, J. Cryst. Growth, 1999, 200, 565.

23 S. Garrault, E. Finot, E. Lesniewska and A. Nonat, Mater. Struct., 2005, 38, 435.

24 J. K. Bates, M. G. Seitz and M. J. Steindler, Nuclear and Chemical Waste Management, 1984,. 5 (1), 63.

25 J. Neeway, A. Abdelouas, B. Grambow, S. Schumacher, C. Martin, M. Kogawa, S. Utsunomiya, S. Gin and P. Frugier, Journal of Non-Crystalline Solids, 2012, 358, 2894.

26 J. Neeway, Ph.D Thesis, University of Nantes, 2010.

27 T. A. Abrajano, J. K. Bates, J. J. Mazer, Journal of Non-Crystalline Solids, 1989, 108, 269.

28 T. A. Abrajano, J. K. Bates and C. D. Byers, Journal of Non-Crystalline Solids, 1986, 84 (1–3), 251.

29 A. Abdelouas, Y. El Mendili, A. Aït Chaou, G. Karakurt, C. Hartnack and J.-F. Bardeau, International Journal of Applied Glass Science, 2013, 4 (4), 307.

30 A. Ait Chaou, A. Abdelouas, Y. El Mendili, R. Bouakkaz and C. Martin, Procedia Materials Science, 2014, 7, 179.

31 W. L Gong, L. M. Wang, R. C. Ewing, E. Vernaz, J. K. Bates and W. L. Ebert, Journal of Nuclear Materials, 1998, 254, 249.

32 David A. McKeown, Andrew C. Buechele, Carol Viragh, Ian L. Pegg, Journal of Nuclear Materials, 2010, 399 (1), 13.

33 David A. McKeown, Andrew C. Buechele, Wayne W. Lukens, David K. Shuh, Ian L. Pegg, Environmental Science and Technology, 2007, 41 (2), 431.

34 Andrew C. Buechele, David A. McKeown, Wayne W. Lukens, David K. Shuh, Ian L. Pegg, Journal of Nuclear Materials, 2012, 429 (1–3), 159.

35 A. Ait Chaou, A. Abdelouas, G. Karakurt and B. Grambow, Journal of Nuclear Materials, 2014, 448 (1–3), 206.

36 K. S. Pitzer and D. J. Bradley, Thermodynamics of High Temperature Brines, in: Lawrence Berkeley Lab., Univ. California, Berkeley, CA, USA, 1979, 40.

37 K. M. Davis and M. Tomozawa, Journal of Non-Crystalline Solids, 1996, 201, 177.

38 K. Ferrand, A. Abdelouas and B. Grambow, J. Nucl. Mater., 2006, 355, 54.

39 A. M. Efimov, V. G, Pogareva and A. V. Shashkin, Journal of Non-Crystalline Solids, 2003, 332, 93.

40 G. Navarra, I. Iliopoulos, V. Militello, S. G. Rotolo and M. Leone, Journal of Non-Crystalline Solids, 2005, 351, 1796.

41 R. Bouakkaz, Ph.D Thesis, University of Nantes, 2014.

42 Ph. Colomban, Journal of Non-Crystalline Solids, 2003, 323, 180.

43 Ph. Colomban and O. Paulsen, Journal of American Ceramic Society, 2005, 88, 390.

44 M. Henry, in B. Silvi and P. D'Arco (eds.), Modelling of Minerals and Silicated Materials, Kluwer Academic Publishers, 2002, 273.

45 D. W. Matson, S. K. Sharma and J. A. Philpotts, Journal of Non- Crystalline Solids, 1983, 58, 323.

46 F. L. Galeener, Journal of Non-Crystalline Solids, 1982, 49, 53.

47 P. McMillan, American Mineralogist, 1984, 69, 622.

48 N. Ollier, Ph.D Thesis, University of Lyon 1, 2002.

49 B. C. Bunker, D. R. Tallant, R. J. Kirkpatrick and G. L. Turner, Physics and chemistry of glasses, 1990, 31, 30.

50 H. Li, Y. Su, L. Li and D. M. Strachan, Journal of Non- Crystalline Solids, 2001, 292, 167.

51 T. Furukawa and W. B. White, Journal of the American Ceramic Society, 1981, 64, 443.

52 B. Gasharova, B. Mihailova and L. Konstantinov, European Journal of Mineralogy, 1997, 9, 935.

53 E. I. Kamitsos, M. A. Karakassides and G. D. Chryssikos, J. Phys. Chem., 1987, 91, 1073.

54 H. Li, P. Hrma, J. D. Vienna, M. Qian, Y. Su and D. E. Smith., Journal of Non-Crystalline Solids, 2003, 331, 202.

55 A. K. Hassan, L. M. Torell, L. Börjesson and H. Doweidar, Physical Review B, 1992, 45, 12797.

56 S. Nonnemenn, Master of Science Thesis, UCF, 2003

57 B.O. Mysen, D. Virgo and C.M. Scarfe, Am. Mineral., 1980, 65, 690.

58 C.-S. Deng, C. Breen, J. Yarwood, S. Habesch, J. Phipps, R. Craster and G. Maitland, J. Mat. Chem., 2002, 11, 3105.

59 S. Martinez-Ramirez, M. Frías and C. Domingo, J. Raman Spectrosc., 2006, 37, 555

60 D. W. Matson, S. K. Sharma and J. A. Philpotts, J. Non-Cryst. Solids, 1983, 58, 323

61 I. L. Botto, V. L., Barone, J. L., Castiglioni and I. B. J. Schalamuk, Mater. Sci., 1997, 32, 6549.

62 J. D. Cotter-Howells, P. E. Champness and J. M. Charnock, Mineral. Mag., 1999, 63, 777.

63 J. A. Ryan, Z. P. hang, D. Hesterberg, J. Chou and D. E. Sayers, Environ. Sci. Technol., 2001, 35, 3798.

64 A. Nakamoto, Y. Urasima, S. Sugiura, H. Nakano, T. Yachi and K. Tadokoro, Mineral. J., 1969, 6 (1-2), 85.

65 J. A. Crowley and N. A. Radford, Mineral. Record, 1982, 13, 273.

66 A. Antonakos, E. Liarokapis and T. Leventouri, Biomaterials, 2007, 28, 3043.

67 H. E. Mason, A. Kozolowski and B. I. Phillips, Chem. Mater., 2008, 20, 294.

68 M. H. Brooker, S. Sunder, P. Taylor and V. J. Lopata, Can. J. Chem., 1983, 61, 494.

69 H. G. M. Edwards, S. E. Jorge Villar, J. Jehlicka and T. Munshi, Spectrochim. Acta. A, 2005, 61, 2273.

70 B. E. Scheetz and W. B. White, Am. Mineral., 1977, 62, 36.

71 C. Slebodnick, J. Zhao, R. Angel, B. E. Hanson, Y. Song, Z. Liu and R. J. Hemley, Inorganic Chemistry, 2004, 43 (17), 5245.